HHS Public Access

Author manuscript

Nat Biomed Eng. Author manuscript; available in PMC 2020 February 19.

Published in final edited form as:

Nat Biomed Eng. 2019 November ; 3(11): 870–879. doi:10.1038/s41551-019-0437-9.

Computationally guided personalized targeted ablation of persistent atrial fibrillation

Patrick M. Boyle[1,2,&], **Tarek Zghaib**[3,&], **Sohail Zahid**[1], **Rheeda L. Ali**[1], **Dongdong Deng**[1], **William H. Franceschi**[1], **Joe B. Hakim**[1], **Michael J. Murphy**[1], **Adityo Prakosa**[1], **Stefan L. Zimmerman**[4], **Hiroshi Ashikaga**[3], **Joseph E. Marine**[3], **Aravindan Kolandaivelu**[3], **Saman Nazarian**[5], **David D. Spragg**[3], **Hugh Calkins**[3], **Natalia A. Trayanova**[1,*]

[1]Department of Biomedical Engineering and Institute for Computational Medicine, Johns Hopkins University, 3400 N Charles St, Hackerman Hall 216, Baltimore, MD 21218, USA.

[2]Department of Bioengineering and Institute for Stem Cell and Regenerative Medicine, University of Washington, N310H Foege, Box 355061, Seattle, WA 98195-5061, USA.

[3]Division of Cardiology, Johns Hopkins University School of Medicine, 1800 Orleans Street Zayed 7, Baltimore, MD 21287, USA.

[4]Department of Radiology and Radiological Sciences, Johns Hopkins University School of Medicine, 601 N Caroline St, Baltimore, MD 21205, USA.

[5]Division of Cardiology, University of Pennsylvania Perelman School of Medicine, 3400 Civic Center Blvd, Philadelphia, PA 19104, USA.

Abstract

Atrial fibrillation (AF) — the most common arrhythmia — significantly increases the risk of stroke and heart failure. Although catheter ablation can restore normal heart rhythms, patients with persistent AF who develop atrial fibrosis often undergo multiple failed ablations and thus increased procedural risks. Here, we present personalized computational modelling for the reliable predetermination of ablation targets, which are then used to guide the ablation procedure in patients with persistent AF and atrial fibrosis. We first show that a computational model of the atria of patients identifies fibrotic tissue that if ablated will not sustain AF. We then integrated the target-ablation sites in a clinical-mapping system, and tested its feasibility in 10 patients with persistent AF. The computational prediction of ablation targets avoids lengthy electrical mapping

[*]Corresponding authors, ntrayanova@jhu.edu.

Author contributions

TZ, PMB, SZ, AP, SN, HGC, and NAT designed the study; PMB, SZ, RLA, DD, WHF, JBH, and MJM conducted simulations and analysed simulation results; TZ, PMB, SZ, RLA, JBH, AP, SLZ, HA, JEM, AK, SN, DDS, HGC, and NAT interpreted imaging and simulation data; HA, JEM, and HGC performed catheter ablation procedures; TZ, PMB, and NAT wrote the paper; HA, JEM, DDS, and HGC edited the manuscript.

[&]These authors contributed equally

Competing interests

NAT, PMB, and SZ are co-inventors in the patent application #15526199 “Systems and methods for atrial fibrillation treatment and risk assessment” (under review).

and could improve the accuracy and efficacy of targeted AF ablation in patients whilst eliminating the need for repeat procedures.

With a prevalence of 1–2% worldwide, atrial fibrillation (AF), an abnormal uncoordinated rhythm in the upper chambers of the heart, is the most common cardiac rhythm disorder and a major contributor to mortality and morbidity[1]. Its burden on the health care system is expected to follow a projected increase in AF prevalence over the coming decades[2]. Patients afflicted by AF have a higher mortality rate due to dramatically increased risk of stroke[1]. AF is also associated with diminished quality of life[3], increased rates of cognitive impairment[4], and high treatment costs[5]. Aiming to achieve a permanent cure from AF, catheter-based radio-frequency ablation uses a catheter inserted into the heart to deliver energy and destroy the ability of cardiac tissue to conduct electrical signals, thus terminating the arrhythmia. The standard-of-care ablation treatment for AF is pulmonary vein isolation (PVI), which encircles the pulmonary veins with lesions, preventing abnormal electric signals generated in the veins from invading the atria[6].

However, in patients with the persistent form of AF (PsAF) who typically develop fibrotic remodelling in the atria[7-10], the mechanisms giving rise to AF shift from electrical abnormality in the pulmonary veins to re-circulating electrical waves perpetuated by the fibrotic substrate[11]. In these PsAF patients, all attempts to target the arrhythmogenic sources in the fibrotic substrate, such as execution of linear ablation lesions across the left atrial roof and mitral valve isthmus and ablations of complex fractionated atrial electrograms, have failed to deliver reasonable outcomes[12], as these approaches do not incorporate strategies for finding the appropriate ablation targets in the atrial substrate on the basis of AF mechanisms. Furthermore, these are all “one-size-fits-all” ablation approaches to treat a disease characterized by high inter-individual variability in fibrosis distribution and, consequently, in the sources that sustain AF[11]. As a result, PsAF patients undergo multiple failed ablations with increasing procedural risks. For these patients there is currently no reliable AF ablation option. Developing and implementing in clinical practice new approaches for ablation of PsAF patients with atrial fibrosis, where the patient-specific AF ablation targets in the fibrotic substrate are determined accurately and reliably, will result in an effective anti-arrhythmia treatment and will spare these patients from increasingly complex repeat procedures, reducing morbidity.

Here, we present the proof-of-concept of a technology for targeted ablation of PsAF patients with atrial fibrosis, where reliable and optimal ablation targets are determined non-invasively by personalized computational modelling pre-procedure and utilized to steer patient treatment. We term this approach OPTIMA: OPtimal Target Identification via Modelling of Arrhythmogenesis. The personalized computational models of the atria are reconstructed from each individual patient’s late gadolinium enhancement magnetic resonance imaging (LGE-MRI) scans. The prediction of the ablation targets in the fibrotic substrate is thus custom-tailored to each patient. Furthermore, as the targets are calculated offline prior to the clinical procedure, the approach avoids lengthy invasive mapping of the patient’s atrial electrical activity. Importantly, the methodology involves a fundamentally new concept: it is designed to completely eliminate the ability of the patient’s fibrotic substrate to sustain AF.

This ablation concept is radically different from any existing AF ablation strategies, as we aim to eliminate not only the clinically-manifested AF, but also latent atrial arrhythmias that could arise from the fibrotic substrate, including those that might emerge following initial ablation. The prospect of uncovering all the potential sources of AF in the patient-specific fibrotic substrate, and not only those that sustain the clinical AF episode, is unique to our personalized modelling prediction of ablation targets. OPTIMA is thus designed not only to make ablation efficacious in PsAF patients, but also to potentially eliminate the need for repeat ablations.

The feasibility of the OPTIMA approach to guide ablation in PsAF patients is demonstrated in a prospective clinical study (n=10). The success of this feasibility study could open the door to means of delivering treatment to PsAF patients and thus chart a pathway for the personalized management of atrial arrhythmia.

The OPTIMA Methodology

A flow-chart of the processes that comprise OPTIMA is illustrated in Fig. 1. The top row of Fig. 1 presents an overview of the approach. For each PsAF patient, a personalized 3D atrial geometrical model is reconstructed from the segmented LGE-MRI prior to the ablation procedure, with representations of both fibrotic and non-fibrotic tissue. Region-specific cell and tissue electrical properties are then assigned to the geometric model. Next, personalized simulations are conducted to determine all the atrial arrhythmias that could arise from the fibrotic substrate; this is done by analysing model responses following rapid pacing from 40 uniformly distributed bi-atrial sites. Based on the model responses, an optimal (minimum-size) set of ablation lesions is determined that fully eliminates the arrhythmogenic propensity of the atrial substrate – these are the OPTIMA ablation targets.

The bottom row of Fig. 1 illustrates the steps undertaken in finding the OPTIMA ablation targets. Analysing the pacing-induced arrhythmias, persistent reentrant drivers (RDs) sustaining AF as well as macro-reentrant atrial tachycardias or flutters (AT/Afl) are determined. The initial set of ablation lesions constitutes the locations of these RDs and, if necessary, ablation lines transecting any macro-reentrant pathways. This set of virtual lesions is then implemented in the model and multisite pacing is repeated to determine whether the lesions render the fibrotic substrate fully non-inducible for atrial arrhythmias. Should new arrhythmias emerge post-virtual ablation (RDs or AT/Afl), the additional targets are determined, and the entire protocol is repeated until complete elimination of the fibrotic substrate's ability to sustain arrhythmias is achieved; that latter represents the hallmark of our approach. In cases where the targets are close to a nearby non-conductive anatomical barrier, they are connected to that barrier via a shortest-distance linear lesion to prevent the formation of AT/Afl[13]. This completes the generation of the personalized OPTIMA ablation target set.

Movie S1 presents a dynamic illustration of all OPTIMA steps. Full description of the OPTIMA methodology, including detail about the simulation procedure, arrhythmia induction and analysis, and ablation targets, is provided in Methods.

Proof-of-concept clinical feasibility study

The proof-of-concept prospective clinical study to demonstrate feasibility of our technology to guide patient treatment was conducted in 10 PsAF patients with atrial fibrotic remodelling. Patients were referred for OPTIMA-guided catheter ablation and underwent pre-ablation LGE-MRI. Patient recruitment and characteristics are described in Table S1. A majority of our PsAF patients (60%) had previously failed catheter ablation procedures (up to three prior ablations) and most of them had co-morbidities (e.g., CHA_2DS_2-VASc score of 2[1;2] (median [inter-quartile range]), mean age of 66±7 years, mean body mass index [BMI] of 30±5kg/m^2).

On the day of the clinical procedure, the custom-tailored OPTIMA targets were loaded into the electroanatomic navigation system in a step-wise process (Fig. 2). This involved segmenting the patient's left atrial (LA) geometry from the magnetic resonance angiography (MRA) scan to construct a 3D surface mesh. Unlike LGE-MRI, the MRA surface shell provides visualization of the PVs, LA appendage, and left lateral ridge needed for navigation during the procedure. Next, OPTIMA ablation targets in the LA were co-registered with the MRA surface shell. The RA surface shell was also co-registered, using affine transformation, with the LA-MRA reference shell. Finally, the LA and RA surface shells with the OPTIMA targets were loaded into the electroanatomical navigation system and displayed in real-time, ready for steer the ablation procedure. Full description of the same-day pre-procedure steps outlined above is provided in Methods. During the procedure, the ablation catheter was steered directly towards the OPTIMA targets without prior mapping. Targets were ablated sequentially.

Determining the OPTIMA targets pre-procedure is illustrated in Fig. 3 for three patients from the 10-patient cohort. Presented are activation sequences during AF and those emerging following the first virtual ablation, as well as the final custom-tailored OPTIMA ablation treatment plans (see also Movies S2-S4). Results for another three patients are presented in Fig. S1. Overall, the first execution of the multisite pacing protocol resulted in 4.5[2.3;6] RDs per model. In one patient (#4), the analysis found no RDs or Afl; accordingly, no OPTIMA-guided ablation was performed. Post-virtual ablation, emergent RDs were observed in three patient-specific models (between 1 and 5 RDs), at locations distinct from those of RDs in the original models. The most common locations of the RDs, including the emergent ones, were the posterior left atrial (PLA) wall (17%), and the left pulmonary veins (LPV) (19%). Combined results of OPTIMA analysis regarding the RDs in all 10 patients are summarized in Table 1. Table S2 details comprehensively the number and location of all RDs, as well as the number of pacing sites from which a given RD was induced. As demonstrated by the data from the OPTIMA analysis presented in Table 1 and Table S2, the RA could also sustain RDs, including emergent ones. This is consistent with the fact that the RAs in the 10-patient cohort displayed significant fibrotic remodelling, of a degree comparable to that of the LAs (18.6±14.2% vs. 24.1±12.4%, Table S1). The total number of RDs (including emergent ones) in the RAs of all patients was 12, while the total number of LA RDs was 32, confirming the higher level of arrhythmogenic propensity in the LA, consistent with previous findings[14,15].

Procedural clinical data from OPTIMA-driven ablation in our feasibility study is presented in Fig. 4 for three patients. Illustrated are locations of LA ablation lesions at the end of the procedure, as rendered in the electroanatomic mapping system, and intracardiac electrograms during the procedure. Additional clinical data for 2 patients is presented in Fig. S2. As the RA is typically not ablated during a routine procedure in PsAF patients, and because this study aimed only to demonstrate feasibility of the OPTIMA approach, physicians' practice played a role; physicians thus sometimes elected to not ablate targets in the RA. Specifically, while 97% of all targets in the LA were ablated (2.5 [2; 4] per patient), only 58% of RA targets were ablated (Table 1 and Table S2). Only one LA target in all 10 patients was not ablated for safety reasons, due to its proximity to the His bundle. Post-ablation, patients were followed prospectively; follow up period was 309[245;386] days. Ablation outcomes data are presented in Table S3.

Conducting the prospective clinical study demonstrated the feasibility of our OPTIMA approach in guiding treatment in patients with PsAF and fibrosis.

Discussion

We have introduced a technology for the targeted ablation of PsAF patients with atrial fibrosis, and demonstrated the feasibility of the technology to guide patient treatment in a prospective study of 10 patients. This is a first-in-human clinical application of an approach that uses simulations conducted in computational models, including patient-specific fibrosis and atrial geometry, to construct specific and detailed ablation plans for each individual.

We used state-of-the-art multi-scale computational modelling to determine non-invasively the optimal set of patient-tailored targets for catheter ablation of the fibrotic atrial substrate; the targets were then incorporated into the clinical procedure, and used to steer patient treatment. By linking the spatial scales, from the cell to the patient atria, the computational prediction of PsAF ablation targets is informed by deep mechanistic understanding[16-18] of how AF dynamics are modulated by the patient-specific fibrotic substrate. OPTIMA-guided ablation embodies the incorporation of cutting-edge biomedical and computational engineering in solving complex clinical challenges in cardiovascular medicine. While there has been another attempt to use personalized computational simulations to guide clinical ablation of AF in patients[19], it involved simulating, on endocardial CT-based LA shell only, a few different template ablation strategies (e.g., PVI only, PVI plus lines, etc.) and empirically selecting the best-performing one to be executed clinically, following the inspection of simulation results. In contrast, the 3D bi-atrial OPTIMA approach targets, in a personalized manner, the RD-sustaining properties of the fibrotic substrate, including those that appear following an initial round of virtual ablations, and is fully integrated in the clinical workflow via co-registration with the electro-anatomical mapping system.

The OPTIMA approach does not use patient-specific electrophysiological parameters in the models; the personalized aspects in the models involve patient-specific atrial geometry and fibrosis distribution. In the current state-of-the-art, personalization of electrophysiological parameters would necessitate invasive data acquisition in each patient. We deliberately avoided the latter in the design of the OPTIMA approach, since non-invasive target

assessment is an advantage of our approach. Inter-patient variability in electrophysiology could affect ablation target location predictions[20]; however, the potential uncertainty in target locations due to the use of average human PsAF electrophysiology is significantly alleviated by the use of virtual ablations and repeated AF inducibility protocols in the models, as we have previously demonstrated[21]. Future advancements in OPTIMA could potentially achieve a more advanced and accurate personalization of the atrial models.

Current AF mapping techniques rely on invasive intra-cardiac manoeuvring of a catheter to hundreds of atrial locations to record, often sequentially and manually, the underlying electrogram characteristics at each site, so that the ablation targets can be determined. Recently, ablation strategies that rely on finding and subsequently targeting substrate RDs have also emerged; these include focal impulse and rotor modulation (FIRM)[22] and noninvasive electrocardiographic imaging (ECGI)[23]. These RD-guided ablation strategies only target RDs that currently manifest in a patient's clinical or induced AF episodes, however, new RDs could arise in the fibrotic substrate after it is modified by the initial set of ablation lesions, leading to AF recurrence[24-26].

The OPTIMA strategy is radically different: it is designed to target all possible RDs, including those that could emerge if the arrhythmia-sustaining propensity of the fibrotic substrate is not eliminated by the initial ablation. When needed, we also incorporate short linear ablations connecting targeted RD sites with the nearest non-conductive anatomical obstacle to prevent macro-reentrant waves from circumnavigating RD ablation lesions, thus decreasing the probability of emergent AT/Afl and arrhythmia recurrence. In its design, the OPTIMA approach represents the most comprehensive PsAF treatment strategy because of its potential to eradicate the ability of the patient's fibrotic substrate to sustain AF, which eliminates the need for repeat ablations. Uncovering all the potential sources of AF in the patient-specific fibrotic substrate, and not only those that sustain the clinically-presenting AF episode, is unique to the computationally-driven OPTIMA approach.

Clinical imaging and OPTIMA simulations revealed that in PsAF patients the RA could also develop fibrotic remodelling and sustain RDs, which could then be targeted for ablation. This underscores the importance of a comprehensive evaluation and targeting of the fibrotic substrate at first ablation in the effort to decrease and even eliminate repeat ablations of increasing difficulty, the latter often resulting in increased morbidity.

As part of the assessment of the feasibility of this technology, we developed an approach to import the OPTIMA targets into the clinical electroanatomical mapping system. Furthermore, the integration of computational heart modelling into the clinical procedure was achieved here within the clinical workflow and timeline. The personalized OPTIMA targets were calculated offline prior to ablation, with all OPTIMA steps being completed within 2.5–5 days based on patient LGE-MRI scans acquired 3–5 days prior to the clinical procedure. Importing the OPTIMA targets into the clinical mapping system was done right before the onset of the procedure, allowing the ablation catheter to be directly navigated to the displayed OPTIMA targets. Thus, our non-invasive approach could provide not only a reliable and accurate prediction of AF ablation targets but could also avoid time-consuming and difficult mapping of atrial electrical activity.

As this is a proof-of-concept feasibility study of a technology and not a clinical trial, it was inherently not designed to evaluate procedural outcomes, moreover that some of the targets in the RA were not ablated. Nonetheless, PsAF did not recur in any of the patients, and only one patient underwent PAF/Afl ablation during the follow-up period (patient #3, Table S3); 44% of patients (4 out of 9) remained on antiarrhythmic drugs. Patient 3 was of very low clinical expectation pre-procedure, as he had the most previous ablations (3), the largest amount of LA fibrosis (46.9%), the largest LA and RA volume indices (87.8 and 74.4 mL/m^2), and the worst CHA_2DS_2-VASc score (5). We view the clinical outcomes here as being considerably better than the standard-of-care AF ablation in PsAF patients, the success rate of which is ~50%[27], although quantitative comparisons cannot be made. To establish the efficacy of the OPTIMA approach in AF suppression in the PsAF population with fibrotic remodelling, a clinical trial with adequate sample size and randomized comparisons will need to be undertaken.

Outlook

Should the OPTIMA approach prove beneficial in a randomized clinical study, it could then transform the management of PsAF patients with fibrosis, a population for whom there is currently no reliable AF ablation option. The ability to non-invasively determine the personalized optimal ablation targets *in-silico* prior to the procedure could spare patients from prolonged intracardiac mapping to probe for potential ablation targets, increased radiation exposure, and potentially arrhythmogenic ablation lesions. If successfully implemented in clinical practice, this approach could be a significant step towards achieving long-term freedom from PsAF while also making ablation procedures more precise and less time-consuming. Finally, our study underscores the potential utility of computational and data-driven approaches in cardiac patient care and exemplifies the trend of merging engineering and medicine towards improving healthcare.

Methods

Patient recruitment.

Ten patients with symptomatic, drug-refractory PsAF who presented to Johns Hopkins Hospital for catheter ablation were included in this prospective study and underwent OPTIMA-guided ablation. All patients provided written informed consent, under a protocol approved by the Johns Hopkins Institutional Review Board, for both the ablation procedure as well as inclusion in medical research at the time of the procedure. Exclusion criteria include: patients with cardiac devices like pacemakers and internal cardiac defibrillators, and with acute or chronic renal insufficiency (glomerular filtration rate <30 ml/min/1.73 m^2); patients who are unable to adhere to the follow-up protocol; patients with contraindication to MRI, including ferromagnetic aneurysm clips, metal in the eye, and implanted ferromagnetic or other MRI-incompatible devices; and patients with a history of allergic reactions to gadolinium-based contrast agents. Table S1 summarizes patients' clinical characteristics. Mean age was 66.1±8.0 years, mean BMI was 29±4 kg/m^2 and 9/10 patients (90%) were men. 6/10 cases (60%) were repeat ablations, with one patient undergoing his

fourth AF ablation. In 3/6 patients who were undergoing repeat ablations, at least one reconnected PV was observed at the time of the OPTIMA-guided procedure.

MRI acquisition.

Images were obtained using a 1.5 Tesla MRI scanner (Avanto, Siemens, Erlangen, Germany) and a 6-channel phased array body coil in combination with a 6-channel spine matrix coil. Contrast enhanced 3D time resolved magnetic resonance angiography (MRA; TWIST, Siemens), obtained immediately following intravenous administration of 0.1 mmol/kg of contrast, was used to define left atrium (LA) and pulmonary vein (PV) anatomy (echo time 1.1ms, repetition time 2.5ms, in-plane resolution 0.7 × 0.7 mm, slice thickness 1.5 mm). To optimize image quality, PsAF patients were kept on anti-arrhythmic medications and/or referred for cardioversion prior to MRI. The MRI examination was performed using the same methodology regardless of the presenting rhythm. In individuals with AF, correlation has been shown between areas of high LGE and fibrotic regions in the myocardium, identified histologically[28] or via intra-cardiac mapping[29].

LGE-MRI scans were acquired within a range of 15–25 (mean 18.8±2.4) minutes following 0.2mmol/kg gadolinium injection (gadopentetate dimeglumine; Bayer Healthcare Pharmaceuticals, Montville, NJ) using a fat-saturated 3D IR-prepared fast spoiled gradient recalled echo sequence with respiratory navigation and ECG-gating, echo time of 1.52ms, repetition time of 3.8ms, in-plane resolution of 1.3 × 1.3, slice thickness of 2.5 mm, and flip angle of 10 degrees. Trigger time for 3D LGE-MRI images was optimized to acquire imaging data during diastole of LA as dictated by inspection of the cine images. The optimal inversion time (TI) was identified with a TI scout scan (median 270ms, range 240–290ms) to maximize nulling of LV myocardium.

Image processing to construct the personalized geometrical model of the of patient atria.

A full description of the geometrical model reconstruction methodology can be found in our prior publications[17,18]. Briefly, epicardial and endocardial contours of the left and right atria were manually delineated using the ITK-Snap software package[30]. For pixels in the transmural space between contours in each slice, fibrotic and non-fibrotic tissue regions were differentiated using the image intensity ratio (IIR)-based approach[29]. The IIR of each atrial wall voxel was calculated by normalizing its LGE-MRI signal intensity to the mean intensity of the LA blood pool. Voxels with IIR>1.22 were classified as fibrotic; we have previously shown that regions with this property correlate to low voltage areas observed during intracardiac mapping[29]. The IIR approach used here has been specifically designed to mitigate the uncertainty in threshold-based methods in segmenting LGE-MRI scans[31] since it uses ratiometric values instead of raw voxel intensities[29].

Shape-based interpolation[32] was used to up-sample segmented images to an isotropic voxel size of 400 μm^3. Next, high-resolution tetrahedral meshes were generated using an established automated approach[33]. These volumetric meshes were 3D, and included atrial wall thickness and the 3D distribution of fibrotic remodelling reconstructed from LGE-MRI. Across all 10 finite-element atrial meshes, average element edge length was 428.4±24.3 μm and the number of nodes ranged from ~1 million to ~2.6 million. These mesh characteristics

are consistent with those reported in previous studies as appropriate for conducting electrophysiological simulations[34,35]. For each atrial model, realistic myocardial fibre orientations were estimated by using a diffeomorphic mapping technique to transform the relevant conductivity tensors from the geometry of an atlas mesh into the patient-specific geometry reconstructed from LGE-MRI, as we have previously described[16,33,36-38]. Volume indices for both atria were obtained by dividing the cavity volume, extracted from each patient-specific model, by body surface area.

In our 3D models, the electrical connection between RA and LA was the inter-atrial septum since the structure and connectivity of inter-atrial conduction pathways (e.g., Bachmann's bundle) cannot be recovered from LGE-MRI scans. Although rule-based methods have been used to impose bundle structures in computational models of the atria[39], we opted not to use this type of approach since we did not want to jeopardize the feasibility of the OPTIMA process to be part of the clinical workflow by adding considerable complexity to the model construction stage. Moreover, while the inclusion of complex intra-atrial structures may change the particular ways in which paced activity devolves into episodes of arrhythmia, it would not be expected to change the specific RD anchoring locations, which are predominantly influenced by the patient-specific pattern of structural remodeling.[16-18]

Modelling of atrial electrophysiology in fibrotic and non-fibrotic regions.

The methodology for computational modelling the electrophysiology of the atria of PsAF patients with fibrotic remodelling can also be found in our published papers[17,18,24,25,40,41]. Specifically, at the cellular scale in non-fibrotic regions, a human chronic AF atrial action potential model[42] with modifications to fit clinical monophasic action potential recordings from patients with AF[43] was used to represent membrane kinetics in each atrial model. This ionic model results in intrinsic action potential duration (APD) that is shorter than that of the normal human atrial action potential. At the tissue scale in the non-fibrotic myocardium, conductivity tensor values (longitudinal: σ_L = 0.126 S/m, and transverse: σ_T = 0.0253 S/m) were calibrated to obtain an effective conduction velocity consistent with the range of values in patients with AF[44] (43.39 cm/s). Test simulations conducted in a regular grid with electrophysiological parameters calibrated using this method showed that longitudinal wavefront conduction in non-fibrotic tissue is in the convergent range (i.e., negligible CV error between coarse and fine finite element meshes with ~100 μm and 400 μm inter-node spacing, respectively).

In the fibrotic regions of the atria, changes to the action potential model were also implemented, as we have described previously[17,18] (+15.4% APD; –49.6% upstroke velocity), representing the effect of elevated TGF-β1, a key component of the fibrogenic signalling pathway. These changes were achieved by reducing three of the underlying ionic currents[45-50] (–50% inward rectifier potassium; –50% L-type calcium; –40% fast sodium current). At the tissue-scale, reduction in conductivity values and charge in anisotropy ratio (σ_L = 0.0547 S/m, σ_T = 0.00683 S/m) represented interstitial fibrosis, gap junction remodelling, and greater impairment of cell-to-cell coupling in the direction transverse to cardiac fibers[51,52].

Analysis of retrospective patient-specific atrial simulations employing this modelling strategy has demonstrated good correlation to clinical results[17,18,24,25,53]. Systematic analysis of pre-ablation ECGI data[53] confirmed our earlier study's mechanistic prediction that RDs dynamically localize to the boundaries of fibrotic tissue clusters[17]. Moreover, using retrospective data from two PsAF patient cohorts at different medical centres, we showed that ablation targets predicted by simulations conducted blindly to results of clinical mapping corresponded to the locations of AF-perpetuating RDs detected by either pre-procedural intracardiac-mapping[24] or ECGI[25].

While in this study we use a set of average human AF electrophysiological properties for non-fibrotic and fibrotic tissue, their distribution is patient-specific. Nonetheless, the lack of full patient-specific electrophysiological properties could bring a level of uncertainty in identifying the OPTIMA targets. The latter was assessed in two sensitivity studies[20,21], which demonstrated that the patient-specific distribution of fibrotic remodelling is the primary factor determining where RDs are anchored in the substrate. The electrophysiological properties determine RD cycle lengths but that does not affect the locations of predicted targets. Nonetheless, changing electrophysiological properties resulted in RDs sometimes relocating to or appearing in other portions of the fibrotic substrate. However, our sensitivity analysis demonstrated that this was mitigated in the OPTIMA workflow by iteratively performing virtual RD ablations until all possible ablation targets are identified. Thus, our approach unmasks all possible locations where RDs could potentially anchor, regardless of the electrophysiological properties.

Simulation of electrical activity and numerical aspects.

The propagation of electrical activity in the personalized atria was simulated by solving the monodomain formulation for representing the spread of current in cardiac tissue using the finite-element method. This system was coupled with ordinary differential and algebraic equations representing myocyte membrane dynamics at each node in the mesh[34]. All simulations were executed using the CARP software package on a parallel computing system[34,54]. A version of this software that is free for academic use is available (https://carp.medunigraz.at/carputils/). Each simulation was run on one standard compute node, each of which was equipped with two Intel Broadwell dual socket, 14-core processors (2.6GHz, 30MB cache) and 128GB of RAM. The compute time required to complete one second of simulation time depended upon the size of the patient's heart and ranged from ~20 to ~80 minutes across all patients (median [inter-quartile range]: 43m03s [37m52s; 51m08s]). The estimated total number of CPU hours for all simulations conducted in all models for this project was approximately 171 full days. Full detail regarding the simulations of electrical activity in cardiac models is found in our recent AF-related publications[17,18] as well as earlier work by our team[33,55,56].

Atrial arrhythmia induction protocol.

As the flow chart of the OPTIMA approach (Fig.1 **top row**) illustrates, each personalized 3D atrial electrophysiological model was used in simulations to determine all the possible arrhythmias that could arise in the given fibrotic substrate. In each patient-derived model, arrhythmias were inducted from 40 pacing sites distributed uniformly throughout the left and

right atria and the results of all 40 distinct simulations (conducted in parallel on a high-performance computing system, as described below) were analysed. The set of 40 pacing sites (see examples in Fig. S4) was picked in each atrial model using an automatic approach that has been shown to reliably produce a desired inter-point spacing[53]. Pacing sites were placed at least 2.5 mm away from the nearest region of dense fibrosis to ensure reliable capture. The distribution of pacing sites throughout the atria covered a large range of potential ectopic foci sites. Importantly, this distribution ensured that we captured all the possible arrhythmias that could arise from the given patient-specific fibrotic substrate; this is an essential feature of the OPTIMA approach. For each pacing site, we ran a simulation that involved applying, at the specified location, a clinically-relevant pacing sequence of 12 electrical stimuli with cycle lengths decreasing from 300 to 150 ms was applied to induce arrhythmias and thus assess the arrhythmogenic propensity of the fibrotic substrate. The protocol was identical to that in our previous publications[17,18].

Notably, since there is no uniformly standardized pacing sequence for inducing AF in the clinic, this protocol is not meant to mimic stimulation that might be applied during an ablation procedure. Rather, it is a sequence that we have found useful for inducing RD-perpetuated AF episodes in atrial models constructed according to our methodology. Following the delivery of the final pacing stimulus, simulations were monitored for self-sustaining electrical wavefront propagation. For all cases in which activity persisted for 5000 ms post-pacing, we applied further analysis to determine whether the cause was an induced RD or macroscopic reentry.

Analysis of pacing-induced atrial arrhythmias.

All pacing-induced arrhythmias were analyzed to determine an initial set of ablation lesions (Fig.1). The analysis consisted of determining the locations of the persistent RDs, as well as any possible macro-reentrant tachycardias. The atrial sites where the persistent RDs were localized were found by determining the RD phase singularity trajectories[57]. The latter were identified using the dynamic wavefront tip trajectory analysis approach[20]. Briefly, RD wavefront “pivot points” were manually identified during a 1000 ms analysis interval at the end of each simulation. This ensured that multiple RD rotations were analyzed and that transient instability immediately following AF initiation was disregarded. In all cases, RDs persisted for at least two rotations and lasted at least 200 ms, which is consistent with the definition of RDs in previous publications[14,58]. While this facilitates straightforward comparison between our study and a standardized clinical approach, in actual fact, most RDs observed in this study were spatio-temporally stable for the duration of the entire 1000 ms analysis interval. Instances of macroscopic reentry (i.e., wavefront propagation around non-conductive obstacles such as the mitral or tricuspid valve annuli) were also identified (RD analysis was not applied in this case).

Determining the OPTIMA ablation targets.

The bottom row of Fig.1 illustrates the steps undertaken in finding the OPTIMA ablation targets. Based on the RD trajectories and macro-reentries identified in each atrial model, initial virtual ablation was performed in each model. Virtual ablation lesions consisted of the tissue volumes within 3.5 mm (i.e., the ablation lesion radius for standard irrigated-tip

catheters)[22] of each RD trajectory; the contained tissue volume was modelled as non-conductive, as in previous simulation studies[18,59]. If episodes of macroreentrant AT/Afl were found, an ablation line transecting the narrowest part of the reentrant pathway between non-conductive barriers was also included (see patient 9 in Fig.2). The arrhythmia-induction pacing protocol was then repeated to determine the emergence of new RDs or macro-reentries; those were then virtually ablated. This process was repeated iteratively until each model was rendered non-inducible for reentrant atrial arrhythmias. To complete the personalized OPTIMA ablation target set, each predicted lesion (based on RD assessment) was connected to the nearest non-conductive anatomical feature (i.e., boundaries of atrioventricular valves or LA/RA veins) via linear lesions (see yellow lines in rightmost column of Fig.2) to avoid creating a new substrate for macroreentrant AT/Afl.

Importing personalized OPTIMA targets into the clinical electroanatomic navigation system.

The OPTIMA ablation target import process involved the following steps: First, the patient's LA geometry was segmented from the MRA scan to construct a 3D surface mesh. Unlike LGE-MRI, the MRA surface shell provides visualization of the PVs, LA appendage, and left lateral ridge needed for navigation during the procedure. Second, OPTIMA ablation targets in the LA were co-registered with the MRA surface shell. Third, since MRA scans do not provide accurate visualization of the RA, a down-sampled RA surface shell was extracted from the LGE-MRI mesh with the OPTIMA targets. Fourth, the RA surface shell was co-registered, using affine transformation, with the LA-MRA reference shell. Fifth, the LA and RA surface shells with the OPTIMA targets were loaded into the CARTO navigation system and merged during the procedure, via the CARTOMERGE module, with a limited electroanatomic map (a 50-point shell) acquired by the mapping catheter, usually of the posterior wall. Multiple independent validation studies have shown that the registration error of the CARTOMERGE system is relatively small (~1–2 mm)[60,61] and the benefit of merging patient-specific imaging with electroanatomic mapping data during conventional AF is well documented [62,63] suggesting that locations displayed in the mapping system correlate well with the actual position of the catheter. In cases where the later-described process failed, a CARTO technician manually annotated the locations of the OPTIMA targets onto the MRA shells.

Ablation Procedure.

Following the import of OPTIMA ablation targets into the electroanatomic navigation system, electrophysiology catheters were advanced under fluoroscopic guidance to the His bundle and coronary sinus in the RA with routine hemodynamic and electrocardiographic monitoring. An intra-cardiac echocardiography catheter was inserted into the RA and assisted in trans-septal puncture. A double trans-atrial septal puncture was performed under fluoroscopic guidance and localization within the LA was confirmed with contrast as well as pressure tracing. Intra-venous heparin was administered to achieve an activated clotting time >350 seconds throughout the procedure. A 3.5-mm irrigated tip with 2-mm inter-electrode spacing ablation catheter (Thermocool Smarttouch, Biosense Webster, Diamond Bar, CA) and a decapolar circular mapping catheter, with 25–15 loop diameter, 8mm inter-electrode spacing (LASSO 2515 Variable Loop Eco Nav, Biosense Webster, Diamond Bar, CA) were

advanced under fluoroscopic guidance to the LA. Pulmonary venous angiograms were then obtained for each of the 4 pulmonary veins. Using circular Lasso catheter, PV electrograms were measured at baseline. In patients undergoing repeat AF ablation, PV-LA electrical reconnections were noted. The limited electroanatomic map of the LA mentioned above, created with the Smarttouch catheter, was registered to the previously segmented LA-MRA shell (including OPTIMA target annotations) using standard landmark-followed by surface-registration techniques. High-output pacing was performed along the anterior aspect of the right PVs to confirm absence of phrenic nerve capture. The oesophagus was marked with a radio-opaque temperature probe for monitoring during ablation. Following OPTIMA-guided ablation, PVI (the standard of care) was performed in all patients.

Prior to the procedure, movies displaying OPTIMA targets with nearby anatomical landmarks annotated were made available to physicians for review and planning. For consistency with previous studies of targeted RD ablation [22], in cases where patients presented in sinus rhythm, AF was induced with burst pacing, and stabilized for at least 10 minutes prior to OPTIMA target ablation. Radiofrequency ablation of OPTIMA targets was performed with the Smarttouch irrigated catheter at the annotated targets using a power of 25W on the posterior wall and 30W elsewhere. OPTIMA targets were ablated sequentially beginning with those corresponding to locations where RDs were induced by a larger number of pacing distinct sites in simulations conducted in the corresponding patient-specific model. Ablation of OPTIMA targets was continued, even in cases where acute AF termination was achieved during the procedure, since the specific purpose of OPTIMA ablation was to eliminate the propensity of the fibrotic substrate to sustain arrhythmias. Energy was applied for 15–30s at each target. No immediate postoperative complications were reported.

Patient Follow-up.

Patient rhythm follow-up consisted of ECGs and clinical evaluation at every 3 months, with ambulatory event monitors as indicated by symptoms.

Statistics.

Results are presented as mean ± standard deviation for variables that are expected to be normally distributed (e.g., patient age, procedure times, extent of atrial fibrosis, etc.); for other variables, median and inter-quartile range are used as summary statistics instead. Categorical variables are expressed as percentages.

Reporting summary.

Further information on research design is available in the Nature Research Reporting Summary linked to this article.

Code availability.

The image processing software ITK-Snap is freely available from http://www.itksnap.org/. Computational meshes are generated using the commercial software Simpleware ScanIP (Synopsis, Inc.). Source code for the human atrial ionic model is freely available from the repository CellML (https://www.cellml.org/, “Exposures: Courtemanche, Ramirez, Nattel,

1998”). All simulations are conducted using the software package CARP, a free version of which can be downloaded for academic use via https://carp.medunigraz.at/carputils/. Simulation results were visualized using either meshalyzer, which can be downloaded via https://github.com/cardiosolv/meshalyzer, or Paraview (Kitware), which can be downloaded via https://www.paraview.org/download/. Data from clinical procedures were visualized using the commercial software CARTOMERGE™ (Biosense Webster).

Data availability.

Relevant data, including patient MRI scans, are available from the authors upon approval from the Johns Hopkins Institutional Review Board.

Supplementary Material

Refer to Web version on PubMed Central for supplementary material.

Acknowledgements

This project was supported by grants to NAT from the NIH (DP1-HL123271); to NAT and PMB from the NIH (U01-HL141074); to PMB from the AHA (16-SDG-30440006); to SN from Biosense Webster; and to SZ from the NSF (graduate fellowship). This project has received funding from the Fondation Leducq (Research Grant number 16 CVD 02). This project was also supported by the Roz and Marvin H. Weiner and Family Foundation; the Dr. Francis P. Chiaramonte Foundation; Marilyn and Christian Poindexter; and the Norbert and Louise Grunwald Cardiac Arrhythmia Research Fund.

References

1. Andrade J, Khairy P, Dobrev D & Nattel S The clinical profile and pathophysiology of atrial fibrillation: relationships among clinical features, epidemiology, and mechanisms. Circ Res 114, 1453–1468 (2014). [PubMed: 24763464]
2. Go AS et al. Prevalence of diagnosed atrial fibrillation in adults: national implications for rhythm management and stroke prevention: the AnTicoagulation and Risk Factors in Atrial Fibrillation (ATRIA) Study. JAMA 285, 2370–2375 (2001). [PubMed: 11343485]
3. Dorian P et al. The impairment of health-related quality of life in patients with intermittent atrial fibrillation: implications for the assessment of investigational therapy. J Am Coll Cardiol 36, 1303–1309 (2000). [PubMed: 11028487]
4. Kalantarian S, Stern TA, Mansour M & Ruskin JN Cognitive impairment associated with atrial fibrillation: a meta-analysis. Ann Intern Med 158, 338–346 (2013). [PubMed: 23460057]
5. Stewart S, Murphy NF, Walker A, McGuire A & McMurray JJ Cost of an emerging epidemic: an economic analysis of atrial fibrillation in the UK. Heart 90, 286–292 (2004). [PubMed: 14966048]
6. Calkins H et al. 2017 HRS/EHRA/ECAS/APHRS/SOLAECE expert consensus statement on catheter and surgical ablation of atrial fibrillation. Heart Rhythm 14, e275–e444 (2017). [PubMed: 28506916]
7. Oakes RS et al. Detection and quantification of left atrial structural remodeling with delayed-enhancement magnetic resonance imaging in patients with atrial fibrillation. Circulation 119, 1758–1767 (2009). [PubMed: 19307477]
8. Marrouche NF et al. Association of atrial tissue fibrosis identified by delayed enhancement MRI and atrial fibrillation catheter ablation: the DECAAF study. JAMA 311, 498–506 (2014). [PubMed: 24496537]
9. Scherr D et al. Five-year outcome of catheter ablation of persistent atrial fibrillation using termination of atrial fibrillation as a procedural endpoint. Circ Arrhythm Electrophysiol 8, 18–24 (2015). [PubMed: 25528745]

10. Xu J et al. Atrial extracellular matrix remodeling and the maintenance of atrial fibrillation. Circulation 109, 363–368 (2004). [PubMed: 14732752]
11. Tanaka K et al. Spatial distribution of fibrosis governs fibrillation wave dynamics in the posterior left atrium during heart failure. Circ Res 101, 839–847 (2007). [PubMed: 17704207]
12. Verma A et al. Approaches to catheter ablation for persistent atrial fibrillation. N Engl J Med 372, 1812–1822 (2015). [PubMed: 25946280]
13. Rappel WJ, Zaman JA & Narayan SM Mechanisms for the Termination of Atrial Fibrillation by Localized Ablation: Computational and Clinical Studies. Circ Arrhythm Electrophysiol 8, 1325–1333 (2015). [PubMed: 26359479]
14. Haissaguerre M et al. Driver domains in persistent atrial fibrillation. Circulation 130, 530–538 (2014). [PubMed: 25028391]
15. Swarup V et al. Stability of rotors and focal sources for human atrial fibrillation: focal impulse and rotor mapping (FIRM) of AF sources and fibrillatory conduction. J Cardiovasc Electrophysiol 25, 1284–1292 (2014). [PubMed: 25263408]
16. Trayanova NA Mathematical approaches to understanding and imaging atrial fibrillation: significance for mechanisms and management. Circ Res 114, 1516–1531 (2014). [PubMed: 24763468]
17. Zahid S et al. Patient-derived models link re-entrant driver localization in atrial fibrillation to fibrosis spatial pattern. Cardiovasc Res 110, 443–454 (2016). [PubMed: 27056895]
18. Zahid S et al. Feasibility of using patient-specific models and the “minimum cut” algorithm to predict optimal ablation targets for left atrial flutter. Heart Rhythm 13, 1687–1698 (2016). [PubMed: 27108938]
19. Shim J et al. Virtual In-Silico Modeling Guided Catheter Ablation Predicts Effective Linear Ablation Lesion Set for Longstanding Persistent Atrial Fibrillation: Multicenter Prospective Randomized Study. Front Physiol 8, 792 (2017). [PubMed: 29075201]
20. Deng D et al. Sensitivity of reentrant driver localization to electrophysiological parameter variability in image-based computational models of persistent atrial fibrillation sustained by a fibrotic substrate. Chaos 27, 093932 (2017). [PubMed: 28964164]
21. Hakim JB, Murphy MJ, Trayanova NA & Boyle PM Arrhythmia dynamics in computational models of the atria following virtual ablation of re-entrant drivers. Europace 20, iii45–iii54 (2018). [PubMed: 30476053]
22. Narayan SM et al. Treatment of atrial fibrillation by the ablation of localized sources: CONFIRM (Conventional Ablation for Atrial Fibrillation With or Without Focal Impulse and Rotor Modulation) trial. J Am Coll Cardiol 60, 628–636 (2012). [PubMed: 22818076]
23. Ramanathan C, Ghanem RN, Jia P, Ryu K & Rudy Y Noninvasive electrocardiographic imaging for cardiac electrophysiology and arrhythmia. Nat Med 10, 422–428 (2004). [PubMed: 15034569]
24. Boyle PM et al. The Fibrotic Substrate in Persistent Atrial Fibrillation Patients: Comparison Between Predictions From Computational Modeling and Measurements From Focal Impulse and Rotor Mapping. Front Physiol 9, 1151 (2018). [PubMed: 30210356]
25. Boyle PM et al. Comparing Reentrant Drivers Predicted by Image-Based Computational Modeling and Mapped by Electrocardiographic Imaging in Persistent Atrial Fibrillation. Front Physiol 9, 414 (2018). [PubMed: 29725307]
26. Lalani GG et al. Organized Sources Are Spatially Conserved in Recurrent Compared to Pre-Ablation Atrial Fibrillation: Further Evidence for Non-Random Electrical Substrates. J Cardiovasc Electrophysiol 27, 661–669 (2016). [PubMed: 26918971]
27. Brooks AG et al. Outcomes of long-standing persistent atrial fibrillation ablation: a systematic review. Heart Rhythm 7, 835–846 (2010). [PubMed: 20206320]
28. McGann C et al. Atrial fibrillation ablation outcome is predicted by left atrial remodeling on MRI. Circ Arrhythm Electrophysiol 7, 23–30 (2014). [PubMed: 24363354]
29. Khurram IM et al. Magnetic resonance image intensity ratio, a normalized measure to enable interpatient comparability of left atrial fibrosis. Heart Rhythm 11, 85–92 (2014). [PubMed: 24096166]

30. Yushkevich PA et al. User-guided 3D active contour segmentation of anatomical structures: significantly improved efficiency and reliability. Neuroimage 31, 1116–1128 (2006). [PubMed: 16545965]
31. Karim R et al. Evaluation of state-of-the-art segmentation algorithms for left ventricle infarct from late Gadolinium enhancement MR images. Med Image Anal 30, 95–107 (2016). [PubMed: 26891066]
32. Raya SP & Udupa JK Shape-based interpolation of multidimensional objects. IEEE Trans Med Imaging 9, 32–42 (1990). [PubMed: 18222748]
33. Vadakkumpadan F et al. Image-based models of cardiac structure with applications in arrhythmia and defibrillation studies. J Electrocardiol 42, 157 e151–110 (2009). [PubMed: 19181330]
34. Plank G et al. From mitochondrial ion channels to arrhythmias in the heart: computational techniques to bridge the spatio-temporal scales. Philos Trans A Math Phys Eng Sci 366, 3381–3409 (2008). [PubMed: 18603526]
35. Niederer SA et al. Verification of cardiac tissue electrophysiology simulators using an N-version benchmark. Philos Trans A Math Phys Eng Sci 369, 4331–4351 (2011). [PubMed: 21969679]
36. Beg MF, Helm PA, McVeigh E, Miller MI & Winslow RL Computational cardiac anatomy using MRI. Magn Reson Med 52, 1167–1174 (2004). [PubMed: 15508155]
37. McDowell KS et al. Methodology for patient-specific modeling of atrial fibrosis as a substrate for atrial fibrillation. J Electrocardiol 45, 640–645 (2012). [PubMed: 22999492]
38. McDowell KS et al. Mechanistic inquiry into the role of tissue remodeling in fibrotic lesions in human atrial fibrillation. Biophys J 104, 2764–2773 (2013). [PubMed: 23790385]
39. Labarthe S et al. A bilayer model of human atria: mathematical background, construction, and assessment. Europace 16 Suppl 4, iv21–iv29 (2014). [PubMed: 25362166]
40. Roney CH et al. Modelling methodology of atrial fibrosis affects rotor dynamics and electrograms. Europace 18, iv146–iv155 (2016). [PubMed: 28011842]
41. Boyle PM, Zahid S & Trayanova NA Towards personalized computational modelling of the fibrotic substrate for atrial arrhythmia. Europace 18, iv136–iv145 (2016). [PubMed: 28011841]
42. Courtemanche M, Ramirez RJ & Nattel S Ionic mechanisms underlying human atrial action potential properties: insights from a mathematical model. Am J Physiol 275, H301–321 (1998). [PubMed: 9688927]
43. Krummen DE et al. Mechanisms of human atrial fibrillation initiation: clinical and computational studies of repolarization restitution and activation latency. Circ Arrhythm Electrophysiol 5, 1149–1159 (2012). [PubMed: 23027797]
44. Konings KT et al. High-density mapping of electrically induced atrial fibrillation in humans. Circulation 89, 1665–1680 (1994). [PubMed: 8149534]
45. Avila G, Medina IM, Jimenez E, Elizondo G & Aguilar CI Transforming growth factor-beta1 decreases cardiac muscle L-type Ca2+ current and charge movement by acting on the Cav1.2 mRNA. Am J Physiol Heart Circ Physiol 292, H622–631 (2007). [PubMed: 16980347]
46. Nattel S, Burstein B & Dobrev D Atrial remodeling and atrial fibrillation: mechanisms and implications. Circ Arrhythm Electrophysiol 1, 62–73 (2008). [PubMed: 19808395]
47. Corradi D, Callegari S, Maestri R, Benussi S & Alfieri O Structural remodeling in atrial fibrillation. Nat Clin Pract Cardiovasc Med 5, 782–796 (2008). [PubMed: 18852714]
48. Pedrotty DM, Klinger RY, Kirkton RD & Bursac N Cardiac fibroblast paracrine factors alter impulse conduction and ion channel expression of neonatal rat cardiomyocytes. Cardiovasc Res 83, 688–697 (2009). [PubMed: 19477968]
49. Kakkar R & Lee RT Intramyocardial fibroblast myocyte communication. Circ Res 106, 47–57 (2010). [PubMed: 20056945]
50. Ramos-Mondragon R, Vega AV & Avila G Long-term modulation of Na+ and K+ channels by TGF-beta1 in neonatal rat cardiac myocytes. Pflugers Arch 461, 235–247 (2011). [PubMed: 21229261]
51. Li D, Fareh S, Leung TK & Nattel S Promotion of atrial fibrillation by heart failure in dogs: atrial remodeling of a different sort. Circulation 100, 87–95 (1999). [PubMed: 10393686]

52. Burstein B et al. Changes in connexin expression and the atrial fibrillation substrate in congestive heart failure. Circ Res 105, 1213–1222 (2009). [PubMed: 19875729]

53. Cochet H et al. Relationship Between Fibrosis Detected on Late Gadolinium-Enhanced Cardiac Magnetic Resonance and Re-Entrant Activity Assessed With Electrocardiographic Imaging in Human Persistent Atrial Fibrillation. JACC Clin Electrophysiol 4, 17–29 (2018). [PubMed: 29479568]

54. Vigmond EJ, Weber dos Santos R, Prassl AJ, Deo M & Plank G Solvers for the cardiac bidomain equations. Prog Biophys Mol Biol 96, 3–18 (2008). [PubMed: 17900668]

55. Boyle PM, Williams JC, Ambrosi CM, Entcheva E & Trayanova NA A comprehensive multiscale framework for simulating optogenetics in the heart. Nat Commun 4, 2370 (2013). [PubMed: 23982300]

56. Arevalo HJ et al. Arrhythmia risk stratification of patients after myocardial infarction using personalized heart models. Nat Commun 7, 11437 (2016). [PubMed: 27164184]

57. Eason J & Trayanova N Phase singularities and termination of spiral wave reentry. J Cardiovasc Electrophysiol 13, 672–679 (2002). [PubMed: 12139290]

58. Narayan SM, Krummen DE & Rappel WJ Clinical mapping approach to diagnose electrical rotors and focal impulse sources for human atrial fibrillation. J Cardiovasc Electrophysiol 23, 447–454 (2012). [PubMed: 22537106]

59. Arevalo H, Plank G, Helm P, Halperin H & Trayanova N Tachycardia in post-infarction hearts: insights from 3D image-based ventricular models. PLoS One 8, e68872 (2013). [PubMed: 23844245]

60. Tops LF et al. Fusion of multislice computed tomography imaging with three-dimensional electroanatomic mapping to guide radiofrequency catheter ablation procedures. Heart Rhythm 2, 1076–1081 (2005). [PubMed: 16188585]

61. Dong J et al. Impact of heart rhythm status on registration accuracy of the left atrium for catheter ablation of atrial fibrillation. J Cardiovasc Electrophysiol 18, 1269–1276 (2007). [PubMed: 17850289]

62. Martinek M, Nesser HJ, Aichinger J, Boehm G & Purerfellner H Impact of integration of multislice computed tomography imaging into three-dimensional electroanatomic mapping on clinical outcomes, safety, and efficacy using radiofrequency ablation for atrial fibrillation. Pacing Clin Electrophysiol 30, 1215–1223 (2007). [PubMed: 17897124]

63. Bertaglia E et al. Image integration increases efficacy of paroxysmal atrial fibrillation catheter ablation: results from the CartoMerge Italian Registry. Europace 11, 1004–1010 (2009). [PubMed: 19541681]

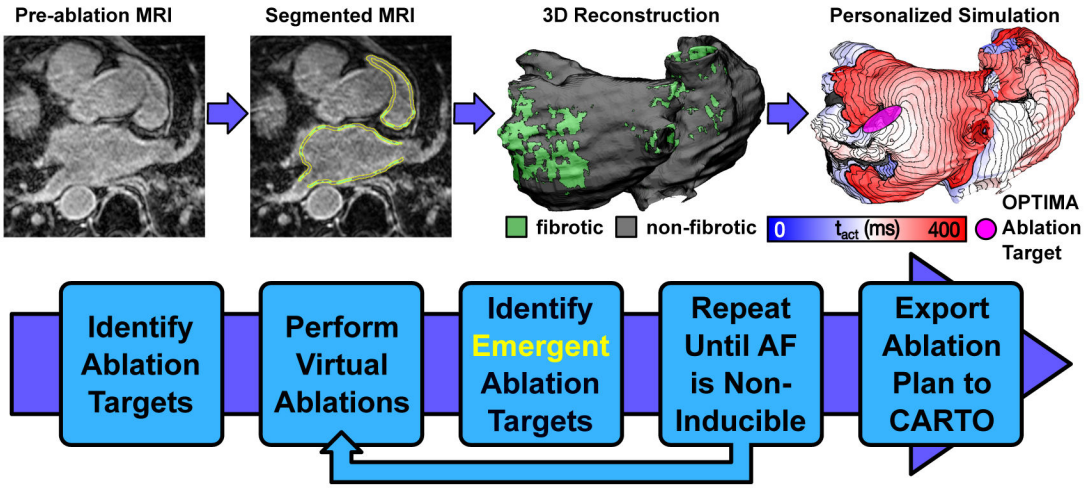

Fig. 1 |. OPTIMA Approach Flowchart.

Top row presents an overview of the approach. Late gadolinium enhancement magnetic resonance imaging (LGE-MRI) scans for each persistent atrial fibrillation (AF) patient are processed to reconstruct a personalized 3D model of the patient's fibrotic atria. Personalized simulations are then conducted to determine all the arrhythmias that could arise in the fibrotic substrate, and the custom-tailored OPTIMA ablation targets are determined. In the final panel of this row, t_{act} indicates activation time. Bottom row presents the detailed steps undertaken in finding the OPTIMA ablation targets based on the arrhythmias that arise in the atrial fibrotic substrate following rapid pacing from 40 uniformly-distributed bi-atrial sites. From the analysis of the pacing-induced arrhythmias, an initial set of lesions is determined, consisting of locations of the persistent reentrant drivers and ablation lines connecting these sites to the closest non-conductive anatomical barriers (pulmonary vein ostia, superior/inferior vena cava openings, or mitral/tricuspid valve annuli). Virtual ablation of these targets is next performed, where the lesions are rendered non-conductive in the model. The rapid pacing protocol is then repeated to determine whether new arrhythmias arise in the post-ablation substrate. The latter two steps are repeated until AF can no longer be induced in the patient's atrial model. Finally, the personalized ablation treatment plan is exported to a format compatible with the CARTO™ system.

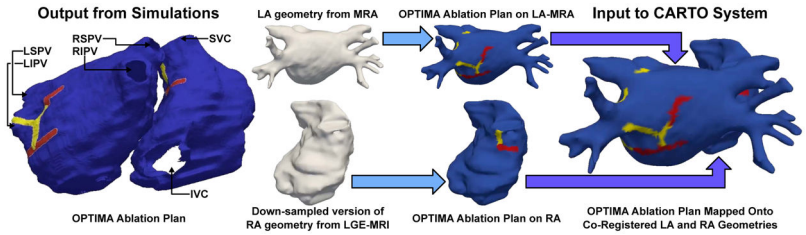

Fig. 2 |. Schematic summarizing the process of importing OPTIMA ablation targets into the clinical electroanatomic navigation system (i.e., CARTO™).

The starting point for this process is the set of outputs from the OPTIMA approach (i.e., ablation targets on bi-atrial volumetric mesh reconstructed from LGE-MRI). Red regions indicate ablation targets from analysis; yellow regions indicate connecting lines. Targets located in the LA are mapped via co-registration onto a geometric reconstruction of the LA endocardial surface extracted from the same patient's MRA scan, which includes anatomical features needed for peri-procedural registration (e.g., prominent ridge between left PVs and lateral LA). Notably, the LA geometry from MRA is a surface mesh (i.e., a 2D manifold in 3D space) and not a volumetric mesh. Since RA segmentation from the MRA scan is not possible, we instead derive a surface mesh of the RA endocardium, including any ablation targets, from the LGE-MRI-based model. The RA surface mesh with ablation targets is then down-sampled since high-resolution meshes cannot be loaded into the clinical mapping system. Finally, the LA-MRA and down-sampled RA surface meshes with the OPTIMA ablation plan are aligned and scale-matched via affine transformation, resulting in a geometric model ready to be converted into a Visualization Toolkit (VTK) file suitable for importing into the CARTO™ system. PV: pulmonary vein; MRA: magnetic resonance angiography; LA/RA: left/right atria; LGE-MRI: late gadolinium enhancement magnetic resonance imaging.

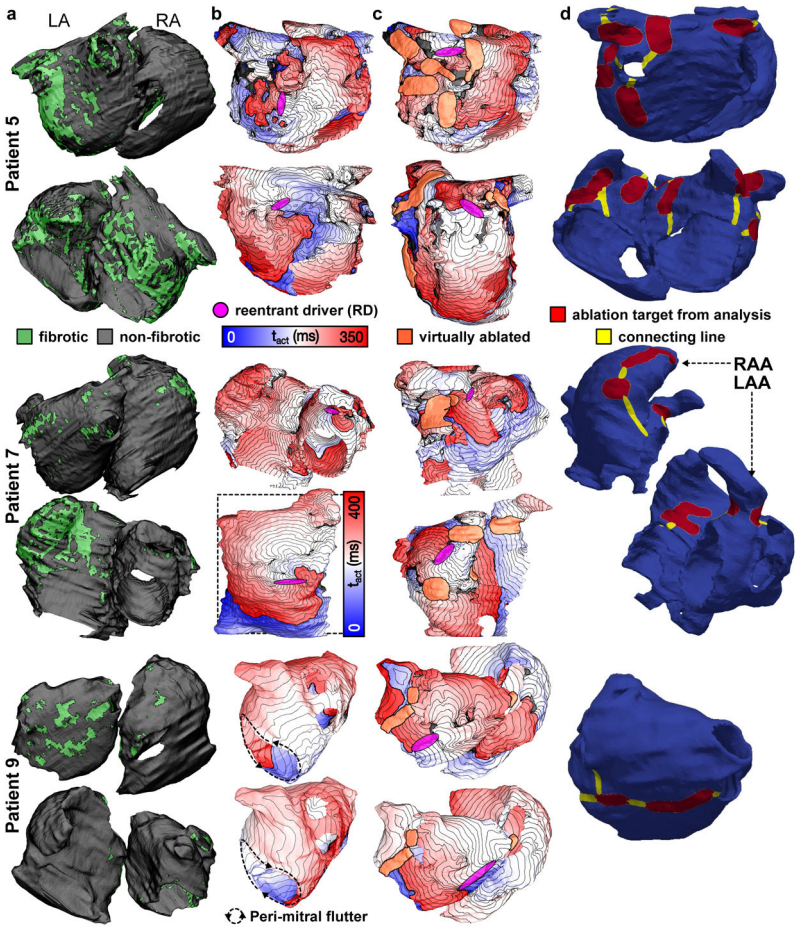

Fig. 3 |.

Examples of the process to determine the OPTIMA ablation targets for three patients. Patient 5, is a 68-year-old man with one prior failed ablation (see also Movie S2). Patient 7 is a 49-year-old man with one prior failed ablation (see also Movie S3). Patient 9 is a 72-year-old man with two prior failed ablations (see also Movie S4). **a,** Posterior (top) and anterior (bottom) views of the three patient-specific atrial models as reconstructed from segmented LGE-MRI scans, including the distribution of fibrotic tissue. **b,** Two examples per model of arrhythmia activation sequences induced by the rapid pacing protocol, and the corresponding persistent reentrant drivers (RDs, pink) obtained from the analysis of the induced arrhythmias. For patient 9, no RD-perpetuated AF was observed following the initial pacing protocol. However, peri-mitral macroreentrant tachycardia was found, and transient episodes of non-sustained reentry were documented in two locations on the posterior left atrium. All activation maps share the same time scale except the lower panel activation map for Patient 7; t_{act} indicates activation time. **c,** Two examples per model of activation sequences associated with arrhythmia emerging anew in the models following virtual ablation (lesions shown in orange), and the corresponding emergent RDs. For patient 9, following virtual ablation to render the initiation of peri-mitral reentry impossible, stable emergent RDs were observed in the same two locations where non-sustained reentries were observed following the initial rapid pacing. **D,** Custom-tailored OPTIMA ablation treatment

plans, including targets corresponding to all RDs (pre-ablation and emergent) and lesion lines connecting the latter to non-conductive tissue boundaries. LA/RA: left/right atria; LAA/RAA: left/right atrial appendage.

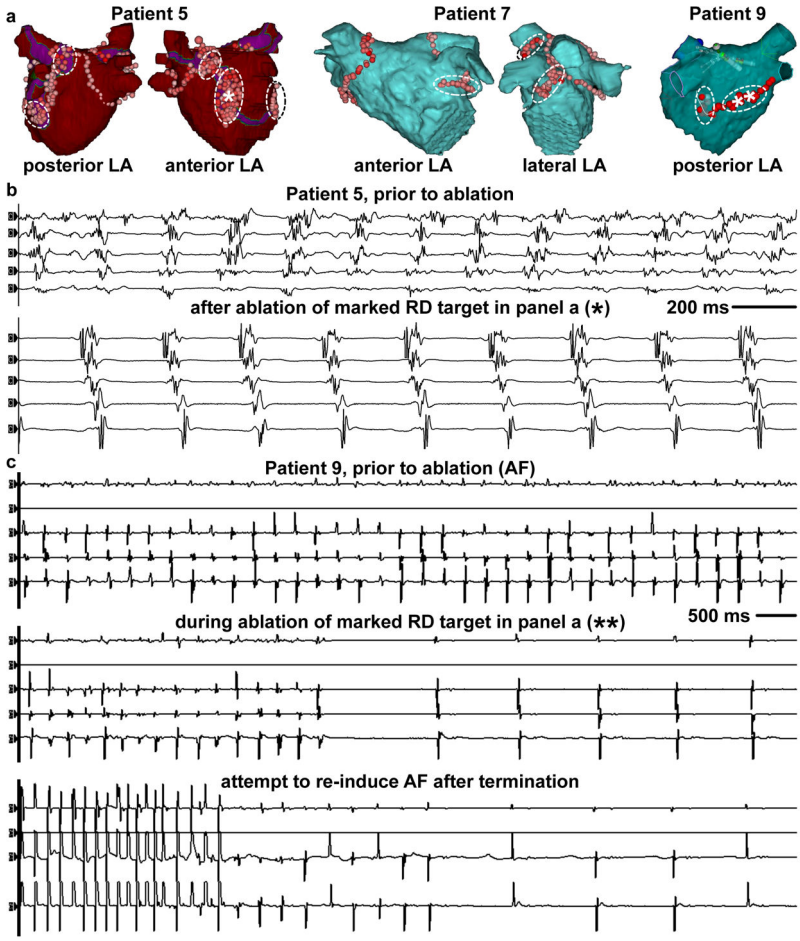

Fig. 4 | Data from the OPTIMA-driven ablation procedures in the three patients from Fig.2. **a,** Sites of ablation delivery (catheter tip locations marked by red dots) in the left atrium (LA) as rendered in CARTO intracardiac mapping system at the end of the clinical ablation procedure in three patients. Dashed ellipses indicate locations ablated based on locations of persistent RDs as identified by OPTIMA. As patient 7 also had targets in the right atrium (RA), Fig. S3 shows the annotated RA CARTO map from the same procedure. **b,** Bipolar electrogram recordings (five per panel) from a decapolar catheter placed in the coronary sinus during the procedure; recordings are from proximal (top) to distal (bottom) leads. Intracardiac electrograms recorded during the ablation procedure in patient 5. Ablation of the marked anterior LA reentrant driver (RD) target (asterisk in a, patient 5) resulted in a transient change from atrial fibrillation (AF) (top row of five electrograms) to an organized atrial tachycardia/flutter (AT/Afl) (bottom row of five electrograms). **c,** Intracardiac electrograms for patient 9. The top panel shows 5 electrograms for patient 9 prior to ablation (AF). Stable induced AF (top row of the middle panel) terminated abruptly (middle row of the middle panel) upon ablation of the marked posterior LA target (** in Figure 4a, patient 9) and AF could not be re-induced despite aggressive rapid pacing (bottom row of the bottom panel).

Table 1 |

Summary of OPTIMA ablation data in all 10 patients.

Summary measures are displayed as median [inter-quartile range]. Of the RDs predicted by modelling, those found in LAA or RAA were not part of the OPTIMA ablation target set imported into CARTO (see Methods), as LAA and RAA ablation is not recommended due to the high risk of stroke. Thus, the total number of model RDs is different from the total number of RD targets in the OPTIMA set. The asterisk * indicates a model RD in LAA or RAA excluded from the OPTIMA set; ** indicates multiple models RDs in LAA or RAA. RD = reentrant driver; LAA/RAA = left/right atrial appendage; LA/RA = left/right atrium.

ID	Total Model RDs (incl. LAA/RAA)	OPTIMA LA RDs	OPTIMA RA RDs	LA Targets Ablated	RA Targets Ablated
1	6	4	1*	4	1
2	1	0	1	0	1
3	8	5*	1*	5	1
5	14	9*	2**	9	0
6	4	2	1*	2	0
7	7	2	4*	2	4
8	6	5	1	4	0
9	2	2	0	2	0
10	5	3*	1	3	0
Total	**53**	**32**	**12**	**31(97%)**	**7 (58%)**
Summary	**5.5 [2.5; 6.75]**	**2.5 [2; 4.75]**	**1 [1; 1]**	**2.5 [2; 4]**	**0 [0; 1]**